

T. L. Delworth · M. E. Mann

## Observed and simulated multidecadal variability in the Northern Hemisphere

Received: 8 June 1999 / Accepted: 11 February 2000

**Abstract** Analyses of proxy based reconstructions of surface temperatures during the past 330 years show the existence of a distinct oscillatory mode of variability with an approximate time scale of 70 years. This variability is also seen in instrumental records, although the oscillatory nature of the variability is difficult to assess due to the short length of the instrumental record. The spatial pattern of this variability is hemispheric or perhaps even global in scale, but with particular emphasis on the Atlantic region. Independent analyses of multi-century integrations of two versions of the GFDL coupled atmosphere-ocean model also show the existence of distinct multidecadal variability in the North Atlantic region which resembles the observed pattern. The model variability involves fluctuations in the intensity of the thermohaline circulation in the North Atlantic. It is our intent here to provide a direct comparison of the observed variability to that simulated in a coupled ocean-atmosphere model, making use of both existing instrumental analyses and newly available proxy based multi-century surface temperature estimates. The analyses demonstrate a substantial agreement between the simulated and observed patterns of multidecadal variability in sea surface temperature (SST) over the North Atlantic. There is much less agreement between the model and observations for sea level pressure. Seasonal analyses of the variability demonstrate that for both the model and observations SST appears to be the primary carrier of the multidecadal signal.

### 1 Introduction

Understanding the internal, unforced variability of the climate system on decadal and longer time scales is of substantial importance to society. Not only does a proper understanding of such variability have significant implications for long-range climate forecasting and societal decision making, but it is precisely these time scales on which anthropogenic impacts on climate are likely to be expressed (Santer et al. 1996). A proper understanding of the internal variability of the coupled ocean-atmosphere system that might be expected in the absence of exogenous climate forcings (both human-induced and naturally occurring, such as variations in volcanic activity or solar irradiance) is critical for the problem of anthropogenic signal detection. Furthering our understanding of such variability is clearly a key focus of current climate research.

The simplest paradigm for interpreting climate variability describes the coupled ocean-atmosphere system as a first-order Markov process (red noise) in which we expect enhanced internal climate variability at progressively longer time scales due to the thermal inertia of the ocean and the associated ‘reddening’ of the stochastic climate spectrum (Hasselmann 1976). Such a model does not predict the existence of peaks in the climate spectrum. While much of the climate system can be explained by this paradigm, there are notable departures from such a model. The El Niño-Southern Oscillation is one well-known phenomenon that leads to greater variability (on interannual, roughly 3–7 year time scales) than would be expected from such a simple conceptual model. Moreover, there appears to be greater variability in the instrumental record than would be expected from simple red (or even “coloured”) noise on both decadal time scales (broadly speaking, 10–20 years, see e.g. Mann and Park 1994, 1996 and the numerous references therein), and multidecadal time scales (broadly, 30–70 years, see e.g. Folland et al. 1984, 1986, 1999; Parker and Folland 1991; Schlesinger and Ramankutty 1994;

---

T. L. Delworth (✉)  
Geophysical Fluid Dynamics Laboratory,  
Route 1, Forrestal Campus, Princeton, NJ 08542, USA  
E-mail: td@gfdl.gov

M. E. Mann  
Department of Environmental Sciences,  
University of Virginia, Charlottesville, Virginia 22903, USA  
E-mail: mann@virginia.edu

Mann and Park 1994, 1996; Minobe 1999). The relevance of this latter multidecadal variability is demonstrated by its use as a predictor in Sahel rainfall forecasts (Folland et al. 1991). In studying the multidecadal variability, however, we are near the limit of what infers the instrumental climate record can provide. Proxy data can be analyzed for a longer-term perspective on multidecadal and century-scale climate variability (e.g. Stocker and Mysak 1992; Mann et al. 1995; Minobe 1997), but that perspective has in the past been hampered by limitations in the spatial extent and reliability of the underlying proxy data. Verifiable proxy based climate reconstructions are, however, now available (Mann et al. 1998), and more robust empirical insight into long-term multidecadal climate variability seems possible (see also Mann 2000).

A complementary approach to such empirical analyses is the use of numerical models of the Earth's climate system. The analysis of extended integrations of such models offers the possibility of detailed analysis of not only the characteristics of model-generated variability but also the underlying physics and potential predictability. An additional benefit of the use of numerical models is the ability to separate a forced signal from internal variability through the use of suitably designed experiments. With only a single realization of the observed climate record this decomposition is problematic. However, there is no guarantee that models can accurately simulate fluctuations in the real climate system.

A combined approach comparing observational (both instrumental and proxy based) and model-based results is therefore highly desirable. Observational analyses provide a powerful constraint on the credibility of model solutions, while the model analyses have the potential to address the underlying physics governing the climate system. Our goal is to provide a direct comparison of observed and simulated multidecadal-to-centennial time scale variability evident in the Northern Hemisphere in instrumental observational studies (Deser and Blackmon 1993; Kushnir 1994; Mann and Park 1994, 1996; Schlesinger and Ramankutty 1994) longer term proxy climate data (Stocker and Mysak 1992; Mann et al. 1995) and coupled ocean-atmosphere model integrations (Delworth et al. 1993, 1997; Timmermann et al. 1998). We make use of recent model-based results, and the proxy based reconstructions of surface temperature patterns during the past few centuries recently estimated by Mann et al. (1998, henceforth 'MBH98') for a more robust, long-term model-data comparison than previously possible. Both the North Atlantic characteristics, and possible larger-scale influences, are investigated.

## 2 Description of observational data and model

### 2.1 Instrumental and proxy based observations

We make direct use of results from recent analyses of instrumental temperature and sea level pressure data to compare with the results obtained in this study. The instrumental analyses are comple-

mented by global surface temperature reconstructions based on "multiproxy" networks of annual resolution proxy climate indicators (dendroclimatic, ice core, varved sediment, coral, and historical indicators, combined with the few available long instrumental records). The temperature reconstructions (MBH98) are based on the annual-mean calibration of such multiproxy networks against the dominant patterns of variation or "eigenvectors" of the twentieth century global surface (land air and sea surface) temperature data, and have demonstrated reconstructive skill in cross-validation with pre-1900 instrumental temperature data. These reconstructions provide estimates of surface air and sea surface temperature over large regions of the globe, based on reconstructions of a lower-dimensional eigenvector-space representation of the global surface temperature field. Inferences from these reconstructions into patterns of past climate variability associated with ENSO (Mann et al. 2000a), and the North Atlantic Oscillation (Mann 2000; Cullen et al. 2000) are discussed elsewhere, as are extensions to the estimation of Northern Hemisphere mean temperatures over the past millennium (Mann et al. 1999). The reconstructed temperature patterns are also available interactively (Mann et al. 2000b). The number of reconstructed eigenvectors decreases back in time (11 back to 1820, 8 back to 1750, 4 back to 1600), thereby leading to a reduction in the degree of resolved spatial variance. The first five eigenvectors resolve approximately 30% of the variance in the twentieth century surface temperature record (12%, 6.5%, 5%, 4%, 3.5%, respectively). The principal eigenvector describes a large share (73%) of Northern Hemisphere mean temperature (and the twentieth century warming trend therein), and can skillfully be reconstructed over the entire past millennium (Mann et al. 1999). The second eigenvector has a close association with ENSO, the third with the North Atlantic Oscillation (NAO), and the fourth and fifth with multidecadal patterns of variability in the Atlantic and elsewhere. The pattern most relevant for describing the multidecadal North Atlantic variability of interest here (the fifth eigenvector) is determined only back to 1650. The limited variance resolved in the proxy based reconstructions at the smallest spatial scales limits a detailed comparison of simulated and observed multidecadal variability. Nonetheless, broad comparison of the spatiotemporal characteristics of modelled and estimated climate variations are possible based on several centuries of data with these reconstructions.

### 2.2 Model output

The primary model output to be used comes from a 1000 year control integration of a coupled ocean-atmosphere model developed at the Geophysical Fluid Dynamics Laboratory (GFDL) described in detail by Manabe et al. (1991, 1992). The coupled model is global in domain, with realistic geography consistent with resolution. The model is forced with a seasonal cycle of insolation at the top-of-the-atmosphere. The atmospheric component numerically integrates the primitive equations of motion using a semi-spectral technique in which the variables are represented by a set of spherical harmonics and by corresponding grid points with a spacing of approximately 7.5° longitude and 4.5° latitude. There are nine unevenly spaced levels in the vertical. The oceanic component of the model uses a finite difference technique with twelve unevenly spaced levels in the vertical, and a horizontal resolution of approximately 3.7° longitude and 4.5° latitude. The model atmosphere and ocean interact through fluxes of heat, water, and momentum at the air-sea interface. In order to reduce climate drift, adjustments to the model-calculated heat and water fluxes are applied at the air-sea interface. These flux adjustments are derived from preliminary integrations of the separate atmospheric and oceanic components (see Manabe et al. 1991, for details). A simple thermodynamic sea-ice model is used, in which the ice moves with the ocean currents.

Preliminary results will also be presented from a 1000 year integration of a recently developed higher resolution version of the model described above. This model (referred to as the R30 coupled model) has approximately twice the horizontal resolution of the

R15 model, a 50% increase in vertical resolution, and also uses flux adjustments. Both models employ similar physics.

### 3 Analyses of the instrumental record

While the length of the instrumental record (100–150 years) is too short for a definitive description of multidecadal variability, recent analyses of the instrumental record do provide some intriguing insights. More than a decade ago, Folland et al. (1984) noted the existence of a distinct multidecadal time scale variation in global SST and marine air temperatures, and later related it to a pattern of pronounced interhemispheric SST contrasts in the Atlantic with strong connections to Sahel drought (Folland et al. 1986, 1991), and possible associations with the El Niño phenomenon. Subsequently Deser and Blackmon (1993) confirmed the existence of similar multidecadal variability in a variety of climate fields in the North Atlantic, and argued for the existence of a cold period in the North Atlantic from about 1900–1930 and a warm period from about 1940–1970. Kushnir (1994, hereafter referred to as K94) analyzed time series of SST spanning the period 1900–1987 over the North Atlantic, and demonstrated that there exists a coherent pattern of SST and associated cold-season half year SLP variations on multidecadal time scales. Cold conditions prevailed around 1920 and in the 1970s to 1980s, while warm conditions prevailed from approximately 1930 to 1960. The spatial patterns of the SST and SLP anomalies span the North Atlantic (see Figs. 5 and 6 of K94), with the largest SST anomalies between approximately 35°N and 70°N. The SLP pattern associated with a positive SST anomaly has an anomalous low pressure centre in the central North Atlantic at about 45°N, with positive anomalies poleward of 60°N. It was speculated in K94 that the observed SLP pattern may be a response to the SST anomaly pattern. The K94 pattern is somewhat different than the NAO atmospheric signal which is clearly seen on the decadal time scale (e.g. Lamb and Pepler 1987; Hurrell 1995).

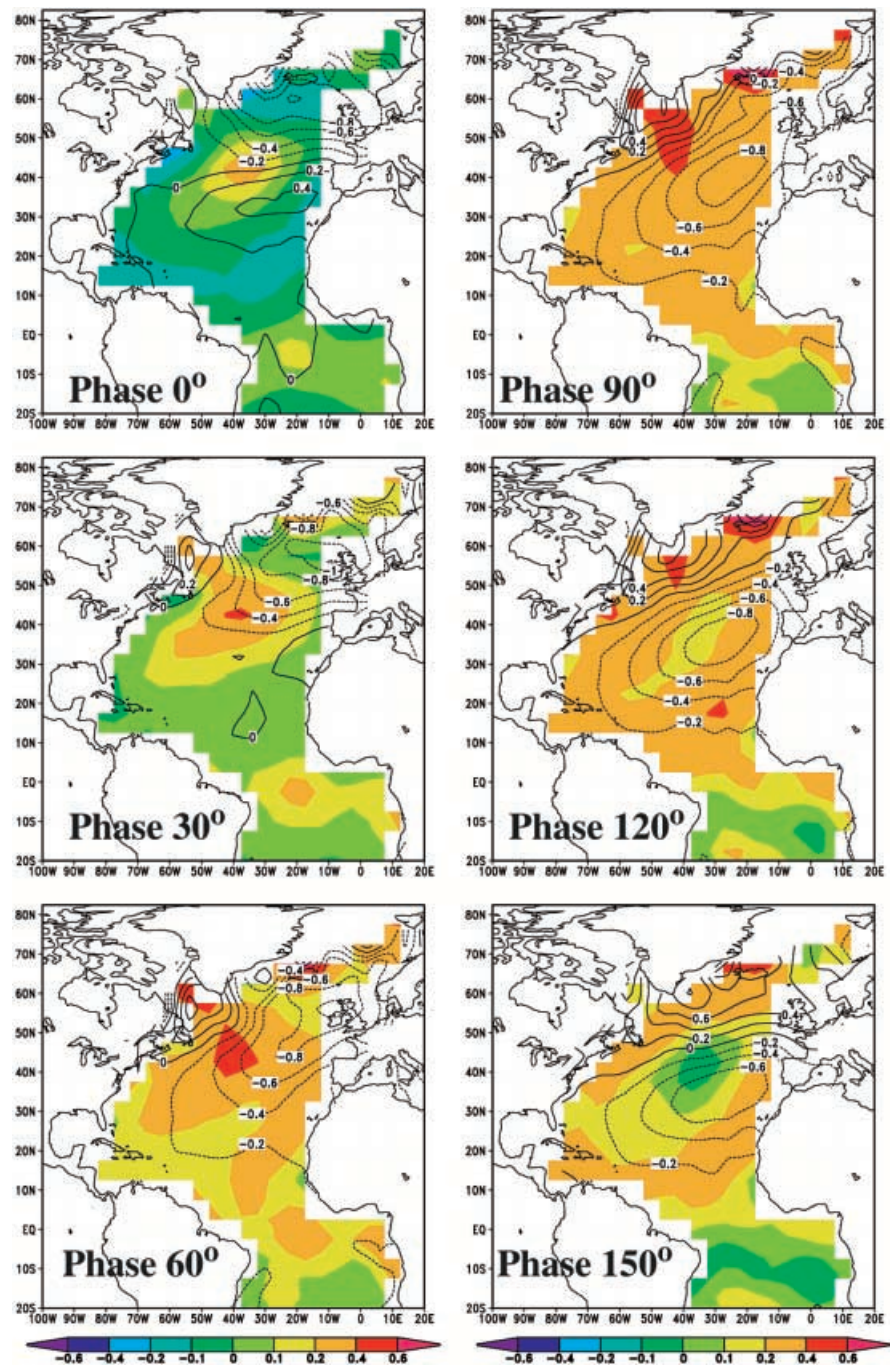
The analysis of K94 was consistent with a coincident study of global-scale temperature signals by Mann and Park (1994, henceforth MP94) which demonstrated a significant multidecadal secular variation in the global temperature record from 1890–1989, largely orthogonal to the principal (global warming) secular variation, but nonetheless statistically significant in its own right. The analysis of MP94 was based on a multivariate frequency-domain method which identifies coherent oscillatory and secular modes of variation (“MTM-SVD”, see the review by Mann and Park 1999, henceforth MP99), and is quite independent of the compositing approach used by K94. MP94 identified apparent larger-scale features of the signal, including opposite sign temperature variations in the South Atlantic (reminiscent of the interhemispheric/Sahel drought-related SST pattern of Folland et al. 1986), and significant amplitude variabil-

ity in parts of the Pacific basin. The pattern nonetheless emphasized the North Atlantic region, and exhibited the “cold-warm-cold” North Atlantic sequence during the twentieth century described by Folland et al. (1986), Deser and Blackmon (1993), and K94. While MP94 noted that this signal resembled a single cycle of a multidecadal oscillation, they emphasized that a true oscillatory signal on this time scale could not be confidently distinguished from a significant secular variation based on a century of data. In an independent study, Schlesinger and Ramankutty (1994) argued that a multidecadal (65–70 year period) signal could indeed be isolated in the global mean instrumental temperature record based on analyses of the nearly 140 year-long IPCC estimated global temperature record (1854–1992).

The MP94 analysis was confirmed and further expanded upon in Mann and Park (1996, henceforth MP96) which used the same method as MP94 to analyze joint fields of SLP and surface temperature in the Northern Hemisphere from 1899–1993, identifying the same multidecadal variation as MP94. That analysis separately analyzed the cold and warm half-year seasonal expressions of the signal, confirming the relationship between SST and SLP identified by K94 during the cold season. Significant impacts on Eurasian cold-season temperatures were inferred as a response to large circulation variations during the cold season over the North Atlantic. The separate cold- and warm-season analyses demonstrated that SST, but *not* SLP, anomalies were seasonally-persistent, suggesting that SST acts as the “carrier” of the signal.

Kushnir et al. (1997) and Tourre et al. (1999) further extended these analyses through the use of a longer instrumental data set based on the Kaplan et al. (1998) statistical reanalysis of SLP and temperature data in the Atlantic region back to 1856. The analysis employed the MTM-SVD technique used by MP94 and MP96, using data long enough to at least marginally resolve a multidecadal oscillatory spatiotemporal signal from secular variability. The authors isolated a spectral peak in the multivariate data fields located in the 50–60 year period range (the associated variance peak maximum is at a 52 year period, although the peak is not clearly resolvable from the secular variance frequency band in this 136 year analysis). The spatial SST and SLP patterns associated with this signal are shown in Fig. 1, adapted from Kushnir et al. (1997). The pattern is consistent in large part with the features of multidecadal variability in the Atlantic discussed involving high-amplitude variability over much of the North Atlantic. The evolving SST and SLP patterns resembled, at certain phases, those in MP96 and K94. The sequence of panels in Fig. 1 denotes the temporal evolution of the pattern at a spacing of approximately 4.3 years. Beginning at phase 0° (defined arbitrarily) in Fig. 1, positive SST anomalies are seen in the central North Atlantic. Positive SLP anomalies are seen in the subtropical North Atlantic, with negative SLP anomalies at higher latitudes of the North Atlantic (this situation resembles a positive phase of the

**Fig. 1** Reconstruction of the approximately 52 year signal in SST and SLP from Kushnir et al. (1997). The *colour shading* denotes SST (units are °C) while the contours depict SLP (units are hPa). *Each panel* is separated in time by approximately 4.3 years. See Kushnir et al. (1997) and Tourre et al. (1999) for details of the analysis



North Atlantic Oscillation). The fact that positive SST anomalies underlie the enhanced westerlies (as inferred from the anomalous SLP gradients) implies that the positive SST anomalies are not being maintained by surface heat flux anomalies induced by wind speed changes, since the anomalous winds should enhance the climatological westerlies and the air-sea heat flux, thereby leading to a cooling of the oceanic surface layer. As we move forward in time to phase 90° (approximately 13 years later), the region of positive SST anomalies expands to encompass the entire North Atlantic, extending to 20°S. This corresponds to the time of

maximum positive SST anomalies in the North Atlantic. There is a distinct shift of the SLP anomalies, such that negative SLP anomalies overlie the positive SST anomalies in the eastern and central North Atlantic, with positive SLP anomalies over the northwest Atlantic.

The Kushnir et al. (1997) findings were independently confirmed by Allan (1999) (see also Folland et al. 1999) based on both MTM-SVD and extended EOF analyses of an independent set of global statistical SST and SLP reanalyses (see Allan et al. 1996) over the world oceans from 1871–1995. The Kushnir et al. (1997) and Allan (1999) analyses emphasize a subtlety to the multidecadal

climate variability that has been obscured in past studies. These latter studies support the existence of a continuously evolving signal, and no analysis of standing patterns of variability can isolate such a signal in its entirety. In the context of this evidence from the extended instrumental record, previous analyses by Folland et al. (1986), Deser and Blackmon (1993), K94, MP94, and MP96, might best be interpreted as having described varying combinations of two orthogonal standing patterns which are in quadrature. The combination of these patterns describes a true multidecadal oscillatory signal with a 50–80 year time scale.

These analyses seem to demonstrate overwhelming evidence for a significant multidecadal variation in the climate system during the past 100 to 150 years, centered in the North Atlantic, but with some degree of global expression. The short nature of these instrumental analyses, however, calls into question whether or not a true multidecadal oscillatory signal can be argued for.

A number of mechanisms have been proposed to account for such multidecadal variability. As discussed in more detail later, internal variability of the coupled ocean-atmosphere-ice system as expressed through variations of the thermohaline circulation (THC) in the North Atlantic has been proposed as a mechanism for this variability (see, e.g. Bjerknes 1964; Stocker and Mysak 1992; Delworth et al. 1993, 1997; Timmermann et al. 1998). It has also been theorized that multidecadal fluctuations of solar irradiance may lead to such variability (Cubasch et al. 1997; Lean and Rind 1998; Waple et al. 2000), either as a direct response to changes in solar forcing, or through some interaction with internal modes of the coupled system. The results to be presented later suggest that temporal variations of the THC present a viable mechanism which could produce multidecadal variability similar to that observed.

## 4 Comparison of observed and simulated multidecadal variability

### 4.1 Analyses using the instrumental record

The Kushnir et al. (1997) and Turre et al. (1999) analyses of the instrumental record can be explicitly compared with analyses of output from millennial-scale integrations of the GFDL coupled ocean-atmosphere model. Previous analyses have demonstrated (Delworth et al. 1993, hereafter referred to as DMS93) that there exists distinct multidecadal variability in this coupled model. The simulated variability involves the thermohaline circulation (THC) in the North Atlantic, has a time scale of approximately 40–80 years, and is associated with SST variations resembling the observed multidecadal SST variations seen in the instrumental record (see Fig. 6 of DMS93 for an explicit comparison). For a more complete discussion of this variability and its mechanism, see DMS93 and Delworth et al. (1997).

In order to make an explicit comparison with the analyses of Kushnir et al. (1997), an MTM-SVD analysis of the combined fields of annual mean SST and SLP is computed for 1000 years of the model output. The spatial domain is similar to that shown in Fig. 1, extending from 45°S to 80°N in the Atlantic. In this analysis, as in all ensuing MTM-SVD analyses, we make the conventional choice (see MP99) of using 3 tapers and a time-frequency bandwidth product  $W = 2N$ , where  $N$  is the length of the data series. This leads to a frequency resolution that is twice as coarse as the nominal Rayleigh resolution of  $\pm 1/N$ , and allows any oscillatory signals with frequency  $f > 2/N$  (i.e. period  $\tau < N/2$ ) to be resolved from a secular trend or variation in the data. The local fractional variance spectrum (LFV, see MP99 for details) is defined as the fractional variance explained by the principal mode in the eigendecomposition as a function of frequency. The LFV spectrum is shown in Fig. 2a, and reveals a clear and significant peak with a time scale of approximately 60 years, similar to the peak in the observed spectrum at 52 years identified by Kushnir (1997) (though, as noted already, the signal time scale is not well constrained in this case. In fact, the underlying signal appears to have a dominant time scale anywhere between 50 and 80 year period, see e.g. MP99).

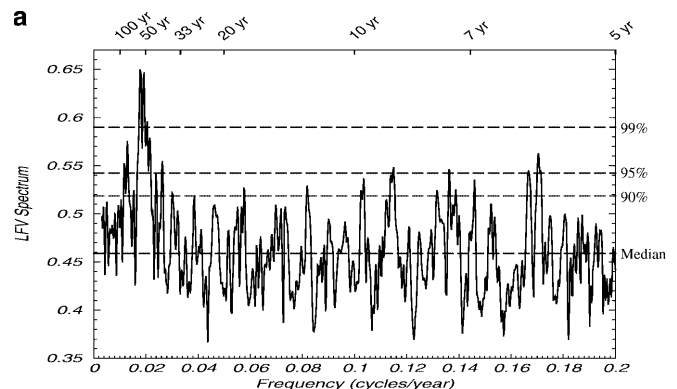
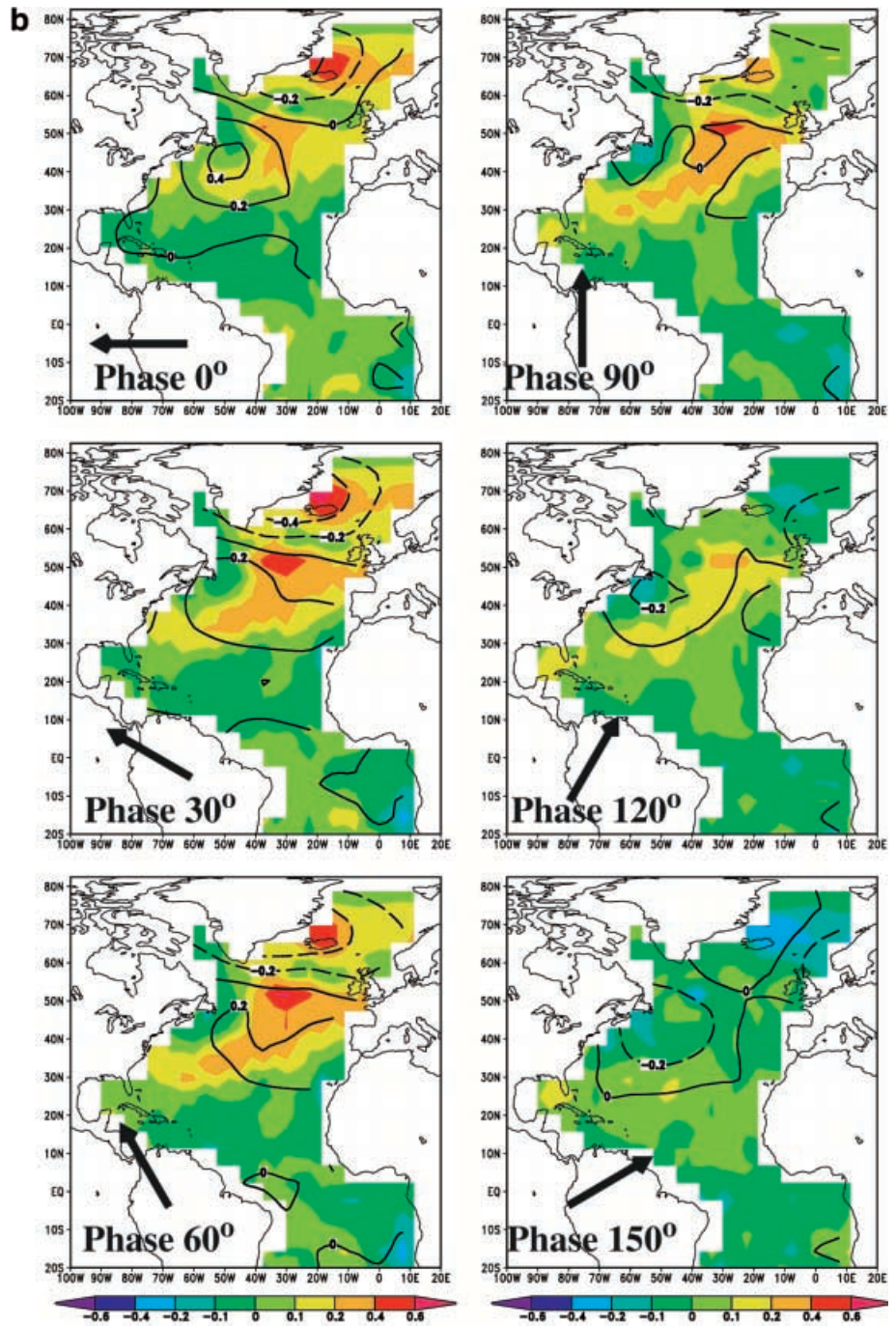


**Fig. 2 a** MTM-SVD LFV spectrum for joint analysis of the model Atlantic SST and SLP fields (45°S to 80°N) in a 1000 year integration of the GFDL coupled model. As in all similar following figures, the secular frequency band (wherein an oscillatory signal cannot be distinguished from a secular variation) is omitted. The periods are listed along the top in years. Shown by horizontal dashed lines are the median, 90%, 95%, and 99% confidence levels for significance relative to the null hypothesis of spatially correlated coloured noise. **b** Spatial pattern of model SST and SLP fields associated with the peak at approximately 56 years in **a**. One half of the full evolution of an approximately 56 year cycle is shown in six equally spaced increments (approximately 4.7 years apart). The colour shading denotes SST (units are °C) while the contours depict SLP (units are hPa). The second half of the cycle (not shown) corresponds to the six panels shown, but with signs reversed for both SST and SLP. The pattern amplitude has been scaled by a factor of 2 as discussed in the text. The arrows in each panel denote the amplitude of the North Atlantic THC at each phase. The upward arrow at phase 90° denotes a maximum positive THC anomaly, while the horizontal arrow at phase 0° indicates an essentially zero anomaly of the THC. A clockwise rotation of the vectors denotes a forward progression in time

Fig. 2b Contd.



In order to compare the spatial patterns of the observed and simulated multidecadal variability, we compute the reconstructed spatial pattern of the signal as it evolves over a typical cycle in each case. The signal pattern is determined based on the approach described by Mann and Park (MP94, MP96, MP99), involving the reconstruction of the principal mode of the MTM-SVD analysis at the central frequency of the observed peak in the LFV spectrum. For the instrumental record (e.g. the Kushnir et al. 1997 analysis shown in Fig. 1), or the proxy reconstructed surface temperature record of the past few centuries (see discussion later), this leads

to a reasonable estimate of the amplitude of a typical oscillation. The MTM-SVD analysis of these surface temperature records, which employ  $N = 136$  and  $N = 330$  years of data respectively, are associated with a maximum frequency resolution of  $\delta f = \pm 0.007$  and  $0.003$  respectively, which either exceeds or is comparable to the intrinsic bandwidth of the 50–70 year period signal ( $bw = 0.008$  cyc/year).

The reconstruction of the spatial pattern associated with the 56 year peak in the model MTM-SVD spectrum is shown in Fig. 2b. In this case, the maximum frequency-resolution in the MTM-SVD analysis of the

$N = 1000$ -year length model fields ( $\delta f = \pm 0.001$ ) is roughly a factor of 4 times finer than the intrinsic bandwidth of the signal (note, e.g. the multiple split peaks in the 50–70 year range in Fig. 2a). The pattern reconstruction at the central frequency of the peak thus potentially underestimates the full signal variance by a factor of roughly four. To adjust for this underestimation, we multiply the pattern amplitude by a corresponding amplitude factor of two for appropriate comparison with the pattern reconstructions shown for the observations. Increasing the amplitude by a factor of two corresponds to a four fold increase in the variance, thereby compensating for the narrow spectral window. Note that another approach to address this issue is to use shorter segments from the coupled model for the reconstructions, thereby using similar spectral windows as the observed data. This technique has also been performed and provides reconstructed amplitudes similar to those shown in Fig. 2b.

Since the signal is cyclical, the beginning phase (defined by phase =  $0^\circ$ ) is arbitrary. We choose to start at the phase of the cycle where SST anomalies over most of the central and northern North Atlantic are positive and increasing. This corresponds to a period preceding the maximum THC in the North Atlantic. This choice is also made to facilitate comparison with the instrumental analyses in Fig. 1, such that a given phase for the model variability corresponds approximately to the same phase for the observational analysis. The phase evolution shown follows one half of a roughly 60 year cycle (the peak is centered at 56 year period), with each  $30^\circ$  phase increment corresponding to approximately 4.6 years. Note that the arrows in Fig. 2b denote the approximate phase of the THC as described in the caption. These phases were determined by matching the SST patterns in Fig. 2b with the spatial pattern of SST obtained by a linear regression analysis between SST and the THC.

Starting at phase  $0^\circ$ , the model has positive SST anomalies in the central and northeastern North Atlantic and Greenland Sea. The simulated SLP pattern has negative values to the southeast of Greenland, with positive values in the west central North Atlantic and central to northern Europe. The general feature of negative SLP anomalies at higher latitudes with positive SLP anomalies in the middle latitudes is in qualitative agreement for that phase with the instrumental analyses shown in Fig. 1. The simulated positive SST anomalies extend further north than the observed anomalies, which are concentrated in the central North Atlantic (Fig. 1, phase  $0^\circ$ ). The SLP pattern for both the observations and the model bears some similarity to a positive phase of the NAO. The model SLP distribution at higher latitudes of the North Atlantic is consistent with anomalous southerly flow over the Greenland Sea (the observational analyses hint at this, but their limited spatial extent precludes a more definitive statement). Additional analyses (not shown; see Delworth et al. 1997) have shown that the simulated East Greenland Current is anomalously weak at this period, thereby

reducing the export of relatively cold, fresh water and sea ice from the Arctic into parts of the North Atlantic. This reduction contributes to the enhancement of the THC by reducing the freshwater transport into the convective regions of the model North Atlantic, thereby effectively increasing near-surface salinity, density, convection, and the THC.

As we proceed forward in the cycle through phases  $30^\circ$  and  $60^\circ$ , we see increasing positive temperature anomalies in the North Atlantic associated with an increasing THC (denoted by the arrows). The model pattern amplifies, with distinct maxima in the SST anomaly pattern in both the central North Atlantic and southern Greenland Sea. This tendency for two maxima in SST anomalies in the North Atlantic and Greenland Sea is also seen in the instrumental analyses at phase  $30^\circ$  and  $60^\circ$ , although the limited spatial extent of the observations limits the analysis to the southern parts of the Greenland Sea. The largest SST anomalies in the model associated with the multidecadal signal are largely confined to the region north of  $20^\circ\text{N}$ , whereas in the observations appreciable SST anomalies extend to  $20^\circ\text{S}$ .

While there is relatively good agreement between simulated and observed temperature at these phases, the SLP fields show distinct differences. The instrumental analyses indicate that the region of negative SLP anomalies appears to move southward with increasing phase, such that by phases  $90^\circ$  and  $120^\circ$  the negative SLP anomalies are centered to the east of the positive SST anomalies at approximately  $40^\circ\text{N}$ . In contrast, for the model the negative SLP anomalies remain fixed in place off the southeast coast of Greenland, and resemble the positive phase of the NAO. The positive SLP anomalies over the North Atlantic tend to shift from west to east.

As we move past phase  $90^\circ$  to phase  $120^\circ$  the simulated and observed SST anomalies begin to weaken. During this period the model THC reaches its maximum, and then begins to weaken, leading to the reduction in SSTs. The maximum SSTs are approximately in phase with the THC maximum, while the subsurface temperature anomalies (not shown) lag the THC by approximately 10 years. The weakening of the simulated THC is related to the presence of an anomalous anticyclonic gyre in the upper 1000 m of the central North Atlantic. The effect of this gyre circulation, induced by positive thermal anomalies associated with the enhanced THC, is to reduce the transport of salt into the convective regions, thereby reducing near-surface density, convection, and the THC (see DMS93). The anomalous model SLP field is still characterized by a north-south pattern, but the amplitudes of the anomalies are somewhat weaker, and the positive SLP anomalies have shifted to the east. The observed SST anomalies reach a peak at phase  $90^\circ$  and decrease thereafter.

As we proceed onward in the model cycle to phase  $180^\circ$  (not shown, but corresponds to phase  $0^\circ$  with signs reversed for both SST and SLP) we see the appearance of negative SST anomalies in the North Atlantic, with

maximum amplitudes at high latitudes. This is associated with a continued weakening of the THC. Note also that by phase  $180^\circ$  there are positive SLP anomalies over Greenland, with negative SLP anomalies over the central North Atlantic and northern Europe. At this phase there are anomalous northerly winds over the Greenland Sea, associated with an enhanced East Greenland Current and enhanced transport of relatively cold, fresh water and sea ice out of the Arctic (see Delworth et al. 1997). This process further weakens the THC by reducing the near-surface density in the convective region. Consistent with this discussion there is good agreement between the simulated and observed variability.

Associated with this phase in the model is a developing cyclonic gyre in the upper 1000 m of the central North Atlantic, related to the cold water associated with the weakened THC and reduced northward heat transport. This cyclonic gyre effectively enhances the transport of salt into the convective regions of the model North Atlantic, thereby sowing the seeds for increased near-surface density, enhanced convection, and a return to a stronger THC over the North Atlantic at a later phase. The intensity of this gyre lags the intensity of the THC by approximately 10 years, thereby contributing to the multidecadal time scale of the oscillation.

It is important to note that while both the simulated and observed SLP anomalies described above bear a resemblance to the NAO at some phases, the full temporal and spatial evolution is more complex than can be described by a single standing pattern. For example, the simulated SLP patterns at both phase  $0^\circ$  and phase  $90^\circ$  would project positively onto the NAO, and yet phase  $0^\circ$  has substantial meridional flow over the Greenland Sea which is not present at phase  $90^\circ$ . Such differences could be very important in modulating the exchange of heat and fresh water between the Arctic and North Atlantic.

#### 4.2 Analyses using the proxy-based reconstruction of surface temperature

The foregoing comparison of the simulated multidecadal variability to the results of instrumental analyses is quite intriguing, but the relative shortness of the instrumental record makes it difficult to draw firm conclusions about multidecadal variability. Indeed, only longer, multiple century empirical records of climate variability can address whether such variations have a distinct time scale and whether they are robust in time. Using such data, Mann et al. (1995) confirmed that a significant multidecadal signal was evident in globally distributed long-term proxy data over several centuries, and the variability had gross spatial features similar to those in the instrumental data. For example, the signal was shown to emphasize the North Atlantic region, and to have larger-scale influences over the Pacific and North American region. The influence of the signal in these latter regions was confirmed subsequently in an independent analysis by Minobe (1997).

In this section we provide an explicit comparison of the multidecadal variability revealed in the comprehensive set of multiproxy-based global temperature reconstructions described in Sect. 2.1 and the GFDL coupled model. MBH98 noted that the multidecadal North Atlantic variation in the instrumental record described by K94, MP94, MP96, Tourre et al. (1999), and others, is largely expressed by the 5th ranked eigenvector of the twentieth century global surface temperature data. It is noteworthy that the expression of the NAO is primarily expressed in an independent (3rd) eigenvector (see MBH98; Mann 1999), and exhibits muted multidecadal variability in comparison. The fifth eigenvector has substantial loadings in the vicinity of the Atlantic basin, and is in general reminiscent of a particular phase of the multidecadal signal established in the instrumental record (i.e. one of the snapshots of the Kushnir et al. 1997 pattern). Though two in-quadrature patterns are required to describe the true multidecadal oscillatory signal (the 4th eigenvector appears to describe much of the in-quadrature pattern during the twentieth century), and the 5th eigenvector almost certainly represents a mixing of the multidecadal signal with unrelated higher-frequency variability, the reconstruction of the 5th eigenvector is available relatively far back in time (AD 1650) making the analysis of its associated reconstructed principal component (RPC) a particularly useful approach to analyzing the robustness of the twentieth century signal back in time. This history is shown in Fig. 3a. Note the clear variations on multidecadal time scales throughout the record, dominated by 50–90 year time scale variability. Indeed, the cold and warm periods identified above in the K94 and other observational studies are readily seen during the twentieth century, but continued cold-warm alterations are clearly evident before 1900. The temporal characteristics of this time series are quantified through a spectral analysis (based on the robust confidence testing approach of Mann and Lees 1996) shown in Fig. 3b. Note the highly significant peak in the 50–100 year band, distinct from secular variability, associated with a persistent multidecadal time scale of variability in the estimated history of the pattern described by the 5th eigenvector. The multidecadal peak is essentially unaltered if the twentieth century variations are excluded from the analysis (see Fig. 3b), demonstrating that the signal is not unique to the twentieth century, but is indeed robust over several centuries. Because the paleoreconstruction approach of MBH98 does not build any a priori frequency domain information from the twentieth century calibration period into the pre-1900 century reconstructions, the latter indications of a multidecadal climate signal are truly independent from any inferences from the instrumental record. These results are consistent with Stocker and Mysak (1992) who demonstrate the existence of distinct multidecadal to centennial variability in a variety of proxy data.

In order to explicitly compare the observed and simulated multidecadal variability, we applied the

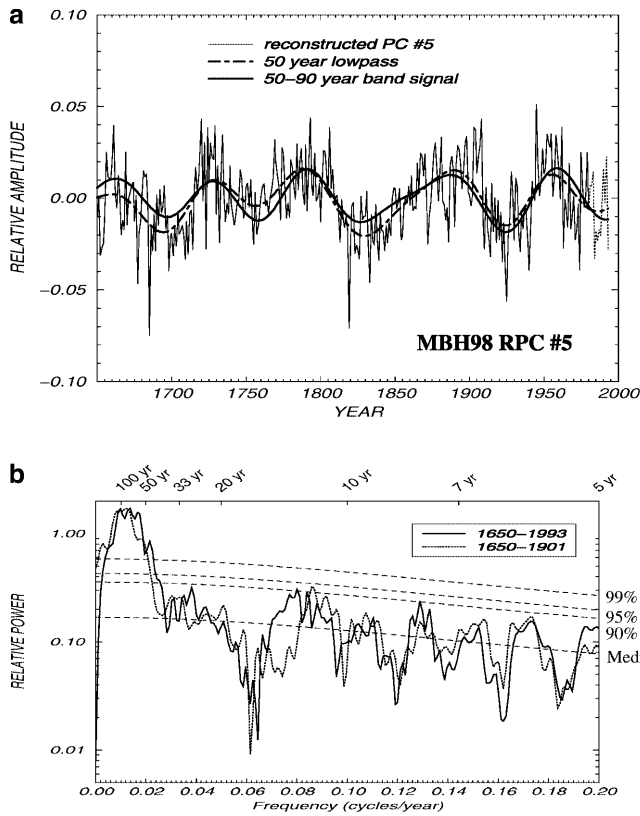


**Fig. 3a, b** Reconstructed principal component (RPC) of Eigenvector 5 from Mann et al. (1998) describing the long-term variations in the dominant surface temperature pattern associated with multidecadal North Atlantic climate variability (refer to Mann et al. 1998, for spatial pattern of this eigenvector). **a** Time-domain signal from 1650–1980 (updated with instrumental PC values after 1980), **b** Multitaper spectrum of the RPC with median red noise background and confidence levels (90, 95, 99%, dashed curves) estimated by the method of Mann and Lees (1996)

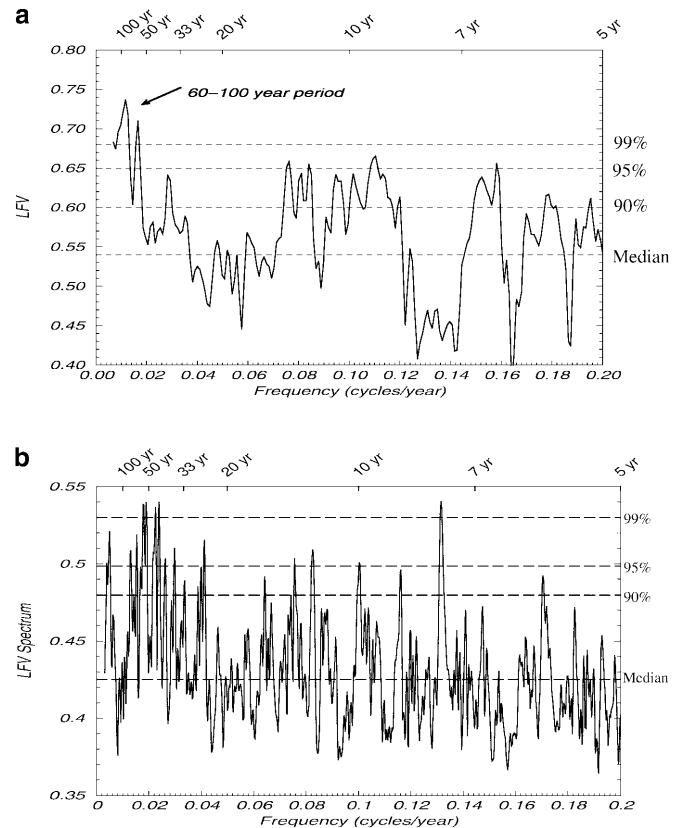


**Fig. 4 a** MTM-SVD LfV spectrum of proxy reconstructed surface temperature patterns (1650–1980) showing highly significant peak centered near 70 year period. Shown by horizontal dashed lines are the median, 90%, 95%, and 99% confidence levels for significance relative to the null hypothesis of spatially correlated coloured noise. The periods are listed along the top in years. **b** MTM-SVD LfV spectrum for joint analysis of the model SST and SLP fields. The domain of analysis for SLP extends from the equator to 90°N; for SST the domain extends in the Atlantic from 45°S to 80°N, and in the Indian and Pacific oceans from the equator to 60°N. Shown by horizontal dashed lines are the median, 90%, 95%, and 99% confidence levels for significance relative to the null hypothesis of spatially correlated coloured noise

MTM-SVD approach (described already) to both the proxy based global surface temperature patterns from 1650–1980 and to 1000 years of model SST. (For the observations, note that prior to 1650 the lack of resolution of the key fifth eigenvector, as discussed in these reconstructions, limits the resolved spatial variance in the temperature pattern reconstructions in the regions of interest.) The model analyses are conducted over the Atlantic from 45°S to 80°N, and over the Indian and Pacific oceans from the equator to 60°N. While the choice of this domain is motivated by the results of previous studies, the sensitivity of the results presented later to the domain of analysis has been evaluated and found to be small. The analyses of the reconstructed data cover approximately the same domain, but have large regions of missing data due to limitations in the reconstruction.

The LfV spectrum (see MP98) for both the observations and model are shown in Fig. 4. The analysis reveals a highly significant peak obtained from the MTM-SVD analysis centered near the 70 year period for the observations and at approximately 56 years for the model. In

both cases the spectral peak exceeds some measures of statistical significance. For the model output the spectral peak becomes much stronger if the domain of analysis is limited to the North Atlantic basin. Separate analyses (not shown) have confirmed that this peak in the model spectrum is strongly related to the described mode of variability of the model thermohaline circulation. Additional analyses using surface air temperature for all model grid points north of 20°S have revealed similar multidecadal variability (results not shown).

The temporal evolution of the patterns of variability associated with the spectral peaks described may be reconstructed (see MP98). These patterns are shown in Fig. 5a for the observational data over oceanic regions. While the loss of spatial variance in the reconstructed patterns for the observations limits any detailed regional inferences, the signal clearly exhibits an evolving spatial pattern (Fig. 5a) during a typical cycle which shares in large part the characteristics of the multidecadal signal

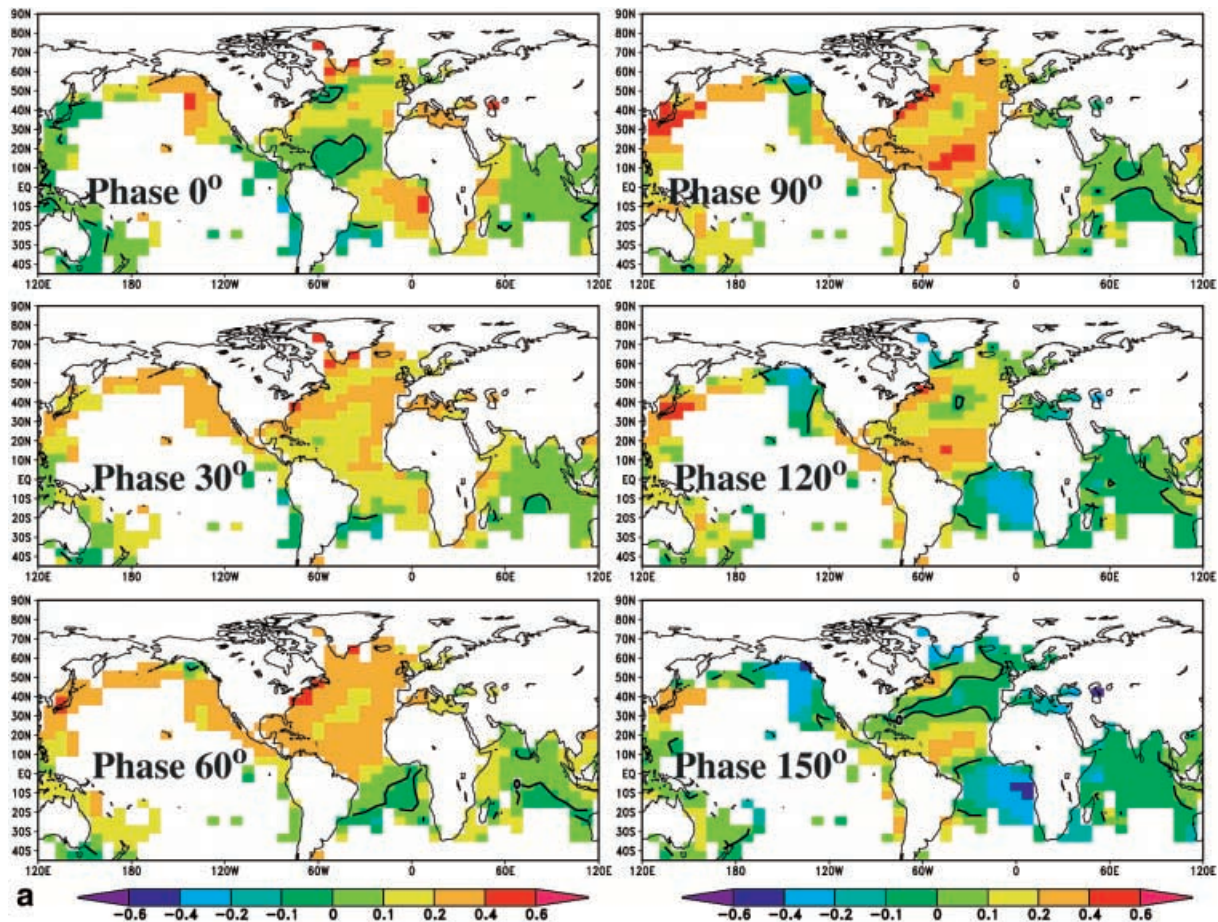


**Fig. 5 a** Spatial pattern of the multidecadal signal in proxy reconstructed temperature identified in Fig. 4a. Shown here is one half of an approximately 70 year cycle in six equally spaced increments (roughly 6 years apart). The other half of the cycle (not shown) would correspond to the same six panels, but with signs reversed (and adding  $180^\circ$  to the indicated phases). Temperatures are *colour-shaded* with the indicated scale, with units of  $^\circ\text{C}$ . The land gridpoints from the MBH98 analysis have been masked out to facilitate comparison with the model results, which are based on SST data only. **b** Spatial pattern

of multidecadal signal in model SST and SLP. Shown here is one half of a typical (56 year) cycle in six equally spaced increments (roughly 4.7 years apart). The other half of the cycle (not shown) would correspond to the same six panels, but with signs reversed (and adding  $180^\circ$  to the indicated phases). Temperatures are *colour-shaded* with the indicated scale, with units of  $^\circ\text{C}$ ; SLP is indicated by the contours (units are hPa), with *dashed contours* indicating negative values. Pattern has been scaled by a factor of two as discussed in text. The *arrows* in each panel denote the phase of the THC as in Fig. 2b

described in the instrumental temperature data. The analysis of this extended proxy reconstructed surface temperature dataset thus points to the existence of a narrowband pattern of variability which has a dominant time scale of approximately 70 years, and which spatially emphasizes the Atlantic and adjoining continental regions.

In order to facilitate the comparison with both the proxy analysis and previously published instrumental analyses, the MTM-SVD analysis was also applied to the joint field of model SST and SLP; the domain of analysis for SLP extends from the equator to  $90^\circ\text{N}$ . Since the spectrum and reconstructed spatial patterns of simulated SST from the joint SST/SLP analysis were extremely similar to those from the MTM-SVD analysis of SST alone (comparison not shown), we have displayed in Fig. 5b the reconstructed pattern of SST and SLP from the joint analysis. In this manner, the SST pattern may be compared explicitly to the proxy temperature

reconstruction in Fig. 5a, while the SLP pattern may be compared to previously published results (e.g. MP96).

Since the signal is cyclical, the beginning phase (defined by phase =  $0^\circ$ ) is arbitrary. We choose to start at a similar phase of the cycle as in Fig. 1, where SST anomalies over large regions of the North Atlantic are positive and increasing. The SST pattern at phase  $0^\circ$  for the model (Fig. 5b) compares reasonably well over the North Atlantic to the corresponding analyses from the multiproxy reconstruction of temperature (see Fig. 5a). In both the model and observations there are positive SST anomalies in the Greenland Sea/northeastern North Atlantic and the central North Atlantic, with a region of negative SST anomalies in the subtropical North Atlantic. There are positive SST anomalies in the eastern south Atlantic in the observational analyses, while the simulated SST anomalies over this region are relatively small.

Over the Pacific the model has positive SST anomalies in the northwestern part of the basin; the proxy

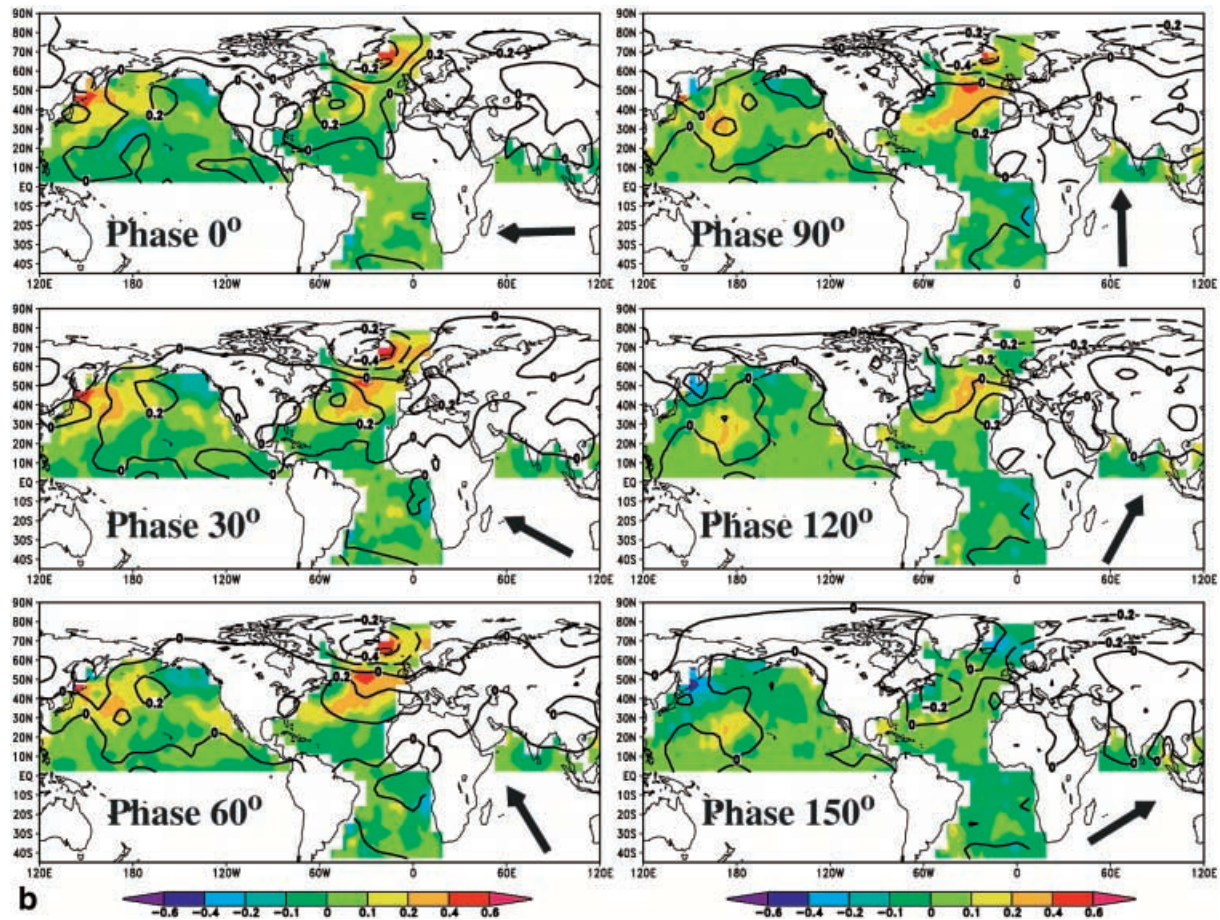


Fig. 5 (contd.)

analysis has positive anomalies in the northern and northeastern parts of the basin.

As we proceed forward in the cycle to phase 90°, we see the largest positive temperature anomalies in the model North Atlantic. During this period the model THC reaches its maximum, and subsequently begins to weaken, leading to an eventual reduction in simulated SST. The temperature anomalies for the proxy reconstruction (Fig. 5a) are also maximum at approximately phase 60°–90°, but their spatial structure is more uniform in the North Atlantic than the simulated pattern. The positive SST anomalies over the South Atlantic in the reconstructions weaken substantially, and become negative by phase 90°. The model has some tendency towards negative SST anomalies over the South Atlantic at this time, but the amplitudes are relatively small.

Over the Pacific both the model and the observations show substantial positive temperature anomalies; for the model the largest values are in the west central North Pacific, whereas the observed values are more homogeneous and cover the northern and eastern sectors of the North Pacific.

There are also positive SLP anomalies over the central North Pacific for the model at this phase. The positive

SST anomalies in the western Pacific are generally in the vicinity of anomalous southerly winds (as inferred from the SLP anomalies). The physical significance of the relationship between the North Atlantic and North Pacific variability in this model is not clear. As will be discussed later, however, Timmermann et al. (1998) postulate an explicit dynamical link between North Atlantic THC multidecadal variations and North Pacific SST and SLP variations based on analyses of an independent coupled model integration. Such a link may depend on the response of the atmosphere to extratropical SST anomalies. It is likely, however, that the link between the North Atlantic and Pacific SLP anomalies is through the atmosphere via teleconnection patterns.

In summary, a direct comparison of the spatial patterns of the simulated and proxy reconstructed observed multidecadal variability has demonstrated some degree of resemblance between the two, with the largest resemblance in the North Atlantic, which is the primary region of the model's multidecadal variability. However, notable differences in the details and amplitudes of the patterns are also clear. For example, the region of large positive SST anomalies over the Atlantic extends much further south in the proxy reconstructions than in the model, consistent with the previously discussed comparison of the model variability to the instrumental analyses.

## 5 Additional characteristics of the simulated multidecadal variability in the GFDL coupled model

### 5.1 Seasonal dependence

It is important to separately examine and compare the cold and warm-season signatures of the model-produced and observed multidecadal signal. Separate analyses of the simulated multidecadal variability using only winter (DJF) and summer (JJA) data are shown in Fig. 6 (only one phase is shown from each season, corresponding approximately to phase 30°–60° from Fig. 5b). It is clear that the SST signal is seasonally invariant. This is consistent with the observational analyses (MP96, see Fig. 5), and supports the notion that the upper ocean is the primary carrier of this multidecadal signal. However, the winter and summer SLP patterns are quite different. Over the North Atlantic, the winter SLP signal has a larger amplitude than the summer signal, and thus dominates the annual mean analyses presented. At this phase, the winter season is characterized by a pattern that has a strong resemblance to the NAO. There is also a smaller positive SLP anomaly in the northeastern Pacific.

During the summer the simulated SLP pattern resembles the observed analyses of MP96 (see Fig. 5c) over the North Atlantic, with anomalously low pressure overlying the positive SST anomaly in the central North

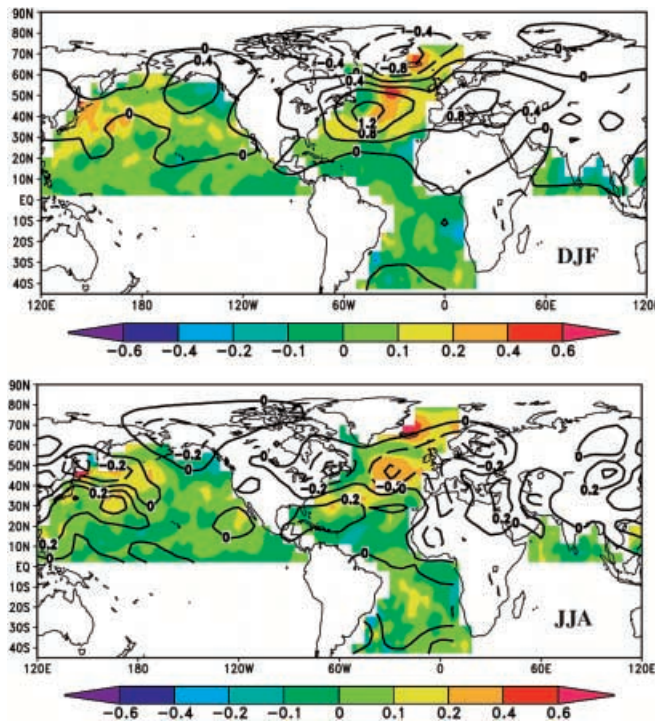


**Fig. 6** Spatial pattern of multidecadal signal in model SST and SLP fields based on seasonal mean analyses (same domain of analysis as described for Fig. 5b). The phase shown corresponds approximately to phase 30°–60° from Fig. 5b. Patterns have been scaled by a factor of two as discussed in text. *Top panel* DJF analysis, *bottom panel* JJA analysis

Atlantic. The summer signal in SLP is approximately 1/3 the amplitude of the winter signal.

We regard the very robust and seasonally persistent expression of the signal in the SST field as the most meaningful surface diagnostic of the dynamics of the signal, related to the underlying oceanic thermohaline circulation dynamics which appear to govern the signal (see DMS93). The precise SLP patterns (and the seasonal details of them) depend on the sensitivity of the overlying atmosphere to extratropical SST anomalies. Such considerations are discussed in more detail later.

### 5.2 Vertical structure

In order to explore the vertical structure in the atmosphere of this mode of variability, additional MTM-SVD analyses were performed on the joint fields of SST, 850 mb geopotential height, and 500 mb geopotential height from the model (the domain of analysis is described in the figure caption). Analyses were performed separately on DJF and JJA mean data, and the results are shown in Fig. 7. The phases displayed correspond approximately to phase 30°–60° in Fig. 5b (as can be inferred from the SST pattern shown in the top panels of Fig. 7). The DJF results (Fig. 7a) show a north-south gradient in anomalous geopotential height over the North Atlantic at both 850 mb and 500 mb, with an approximately 50% increase in amplitude between the two levels. Over the Pacific the spatial pattern of the anomalous geopotential heights is similarly invariant with height, and there is a similar increase of amplitude with height. Thus, one could describe the DJF atmospheric anomaly structure as equivalent barotropic, similar in this respect to the observed Arctic Oscillation (Thompson and Wallace 1998).

The results from JJA are somewhat different. As described in the previous section the amplitudes of the atmospheric anomalies in JJA are considerably weaker than in DJF, with a rather different spatial structure. There is some tendency of the anomalies to amplify with height.

### 5.3 Ocean-atmosphere coupling

A key issue is whether the simulated THC multidecadal variability is due to a coupled air-sea mode of variability, or whether it is due to internal oceanic variability. For our purposes we regard a coupled mode as variability arising from a process in which the large-scale state of the ocean (SST) strongly influences the large-scale state of the atmosphere, which in turn feeds back coherently upon the state of the ocean. A clear example of this type of variability is the El-Nino-Southern Oscillation (ENSO) in the tropical Pacific. DMS93, along with Griffies and Tziperman (1995), speculated that the multidecadal THC variability was primarily due to internal oceanic variability stimulated by stochastic

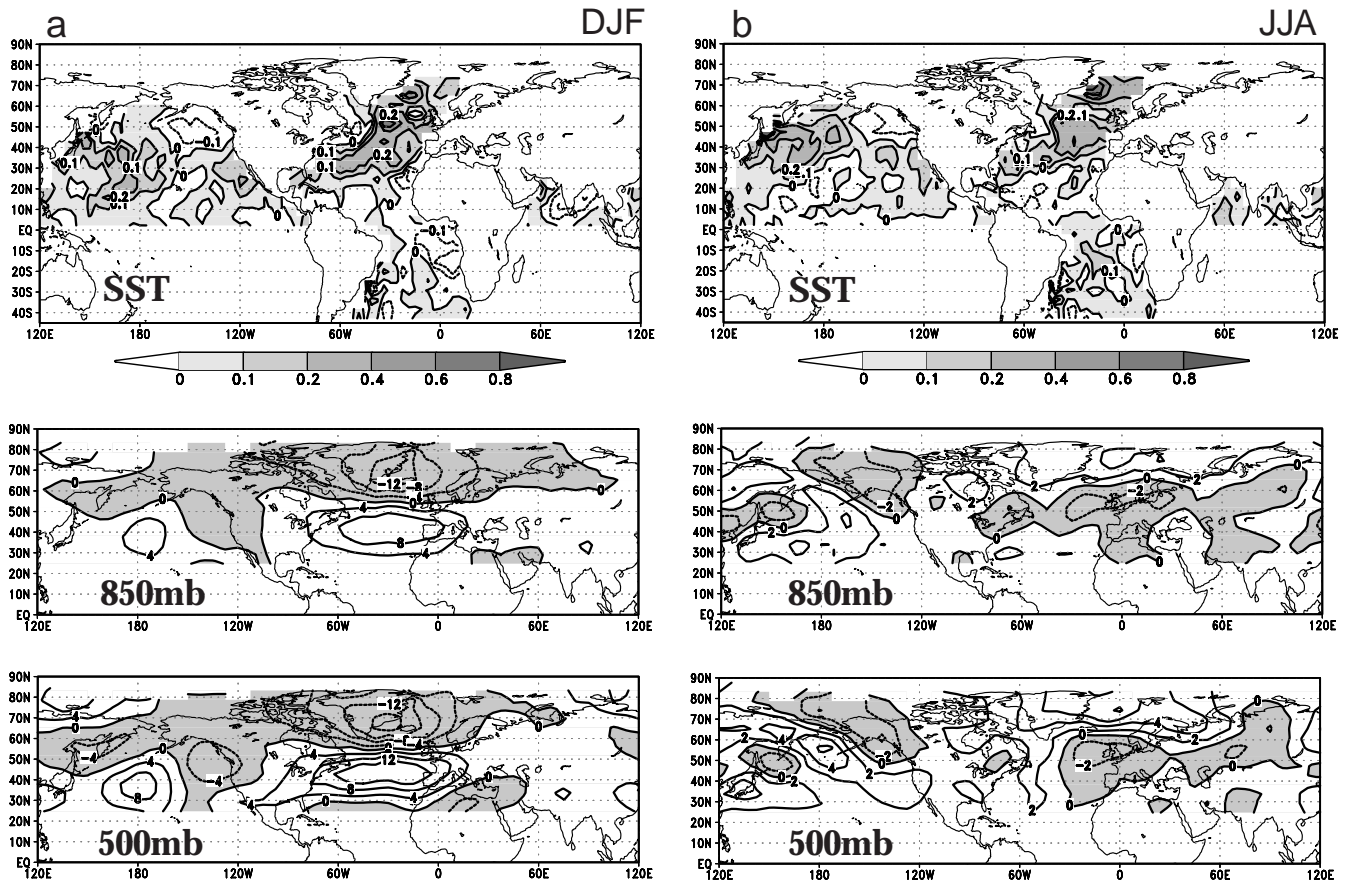


Fig. 7a, b Spatial pattern of multidecadal signal from a joint analysis of annual mean SST, 850 mb geopotential height and 500 mb geopotential height. The domain of analysis for SST is identical to that described in Fig. 5b, while the domain for geopotential heights extends from 20°N to 90°N. The phase shown corresponds

approximately to phase 30°–60° from Fig. 5b. This analysis indicates the vertical structure in the atmosphere associated with the multidecadal variability. Patterns have been scaled by a factor of two as discussed in text. **a** Analysis using DJF data; **b** analysis using JJA data

surface fluxes. Delworth and Greatbatch (2000) have run a number of experiments using the ocean component of the GFDL coupled model. They demonstrate that much of the THC variability can be generated by surface flux forcing which is stochastic in time, thereby suggesting that the variability does not depend critically on the existence of a coupled mode (as defined already). In fact, given the very weak response of the atmospheric model used in DMS93 to mid-latitude SST anomalies (see Kushnir and Held 1996) it would be surprising if a coupled air-sea mode in the mid-latitudes could be supported in this model. Further, Delworth and Greatbatch (2000) show that surface heat fluxes (rather than momentum or fresh water) are the dominant fluxes in exciting this variability. Delworth and Greatbatch (2000) do show, however, that air-sea interactions are very important in determining the magnitude of the surface heat flux anomalies, and thus of the THC variations.

The MTM-SVD analysis further reinforces the notion of an oceanic “carrier” of the multidecadal signal. A separate analysis of the SLP and geopotential fields alone (not shown) yields no statistically significant peak

in the multidecadal period range of interest. In contrast, analyses of both the SST field alone, and joint SST/atmospheric fields, show a consistent significant multidecadal signal. Moreover, the SLP fields associated with the signal do show a consistent though seasonally specific relationship with the SST field, and the SLP expression of the signal cannot be dismissed as random. The sum of these results is thus best interpreted as indicating an oceanic signal, any particular phase of which favours the projection of a particular resonant pattern from an essentially white-noise atmospheric background, the magnitude of which is weak enough relative to noise levels that the signal cannot be clearly detected in the atmospheric fields alone.

## 6 Results from additional coupled models

In order to assess the dependence on resolution of the simulated multidecadal variability, an MTM-SVD analysis was conducted using recent results from a 1000 year integration of the GFDL R30 coupled model. Shown in Fig. 8 is the MTM-SVD LFV spectrum of the

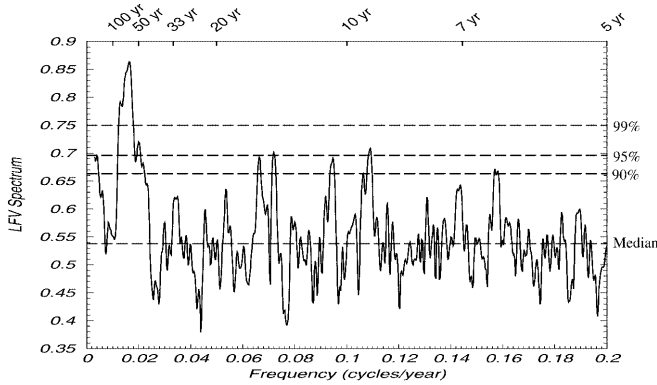


**Fig. 8** MTM-SVD LfV spectrum for SST from the R30 coupled model. The domain of analysis extended in the Atlantic from the equator to 80°N. The analysis used 700 years of annual mean data from the model. Shown by horizontal dashed lines are the median, 90%, 95%, and 99% confidence levels for significance relative to the null hypothesis of spatially correlated coloured noise

model SST field computed from model years 301–1000 using a domain in the North Atlantic from the equator to 80°N. There is a very clear peak on time scales which are similar to the peak in the R15 model, thereby demonstrating similar variability in two models of quite different resolution, but similar physics. Additional analyses (not shown) have revealed that this spectral peak is related to fluctuations in the THC.

The presence of multidecadal THC variability is not unique to the GFDL coupled model. Timmermann et al. (1998) have demonstrated that a distinct mode of multidecadal variability of the THC exists in the ECHAM-3 coupled model at the Max Planck Institute. In an extended control integration of that model they report variations of the THC with an approximate time scale of 30–35 years (distinctly shorter than in the GFDL model). The mechanism for their variations depends on two-way interactions between the atmosphere and the ocean. The spatial patterns of SST, SSS, and SLP anomalies associated with this variability bear a strong resemblance to the GFDL model results (for example, compare Fig. 14 of Timmermann et al. 1998, to Figs. 6 and 20 of DMS93). There are also some differences; Timmermann et al. (1998) report a large-scale response of the atmosphere to thermohaline-related SST variations in the Atlantic which encompasses the entire Pacific/North American sector, whereby coupled ocean-atmosphere processes in the North Pacific take on, at least, a secondary role. The latter connection is intriguing in that it is consistent with studies (MP94; Mann et al. 1995; MP96; Minobe 1997) which argue for a detectable multidecadal signal in the North Pacific. Kushnir and Held (1996) note, however, that the GFDL low-resolution atmospheric model exhibits little evidence of sensitivity of the overlying atmosphere to mid-latitude SST anomalies, in contrast to the MPI coupled model. This distinction probably explains why a much larger-scale resonant barotropic response to North Atlantic SST is observed in the MPI multidecadal signal, but not in

DMS93. Kushnir and Held (1996) question the robustness of such a barotropic response, and point out that the matter of which response is physically correct is not yet resolved. In spite of these differences in atmospheric sensitivity, however, the agreement in SST and SLP between the two models is quite good.

An additional extended integration of a coupled model in which there is substantial THC variability on multidecadal time scales is reported by Capotondi and Holland (1998). They show that in a 300 year integration of the NCAR Climate System Model (CSM) there are distinct variations in the intensity of the THC with a 30 to 50 year time scale, along with associated spatial patterns of SST and SSS anomalies which resemble the GFDL results. Their conclusion is tempered, however, by the relatively short integration.

Recent analyses (Vellinga and Wood 1999) of a multi-century control integration of the Hadley Centre HADCM3 coupled ocean-atmosphere model show pronounced multidecadal variability in volume transport across a section south of Greenland. These results are of particular importance because of the relatively higher resolution of that model.

These results suggest, at a minimum, that the existence of distinct multidecadal time scales of variability in the North Atlantic is not unique to the GFDL coupled model. Such multidecadal variability is particularly relevant in light of model projections of future reductions in the intensity of the THC due to increasing concentrations of greenhouse gases in the atmosphere (Manabe and Stouffer 1994; Haywood et al. 1997; Wood et al. 1999; Dixon et al. 1999).

## 7 Summary and discussion

Our purpose has been to compare results from analyses of both the instrumental and proxy climate record with the output from extended integrations of coupled ocean-atmosphere models. We wish to see to what degree recently documented multidecadal variability in the North Atlantic agrees with simulated multidecadal variability in coupled ocean-atmosphere models.

Recent analyses of both the instrumental record and an extended record derived from multiproxy data have shown a distinct pattern of multidecadal variability encompassing the North Atlantic region. The instrumental record has revealed basin-wide patterns of SST changes associated with large-scale SLP anomalies. An extended multiproxy record representing surface temperature has shown that such multidecadal variability has been present in the climate system over the last 300 years.

Several recent extended integrations of coupled ocean-atmosphere models have been shown to contain multidecadal variations of the thermohaline circulation in the North Atlantic. Associated with these variations are large-scale anomaly patterns of sea surface temperature (SST) and sea level pressure (SLP) which resemble the results from observational analyses. However, there

is an apparent phase difference between the SLP patterns for the observations and the models.

One of the principal issues with regard to climate variability on these time scales involves the relative interactions between the oceanic circulation and the atmosphere at mid-latitudes. The work of Timmermann et al. (1998) suggests that a relatively strong response of the atmosphere to extratropical SST anomalies gives rise to a coupled mode of variability encompassing both the thermohaline circulation in the North Atlantic and the North Atlantic Oscillation. The work of Delworth et al. (1993) and Delworth and Greatbatch (2000), however, suggests that such multidecadal variability in the THC can arise as an oceanic response to stochastic surface flux forcing. In reality both processes can be operating. It is thus of paramount importance to increase our theoretical understanding of the atmospheric response to SST anomalies at mid-latitudes (Latif, 1998).

A fruitful path towards improving our understanding of decadal to centennial climate variability lies in close comparisons between observed and simulated climate variations. The analyses presented here are a step along this path. While the models used in this study have fairly coarse resolution and simplified physics, they nonetheless successfully simulate many aspects of the Earth's climate. In addition, these same properties allow multiple extended integrations with available computing resources. There are also substantial limitations with regard to the instrumental and proxy data, including limitations in both spatial and temporal coverage. Thus, it is clearly desirable to improve both the models and the available data in order to further our understanding of this topic.

**Acknowledgements** We thank S. Griffies, J. Lanzante, S. Manabe, R.J. Stouffer, and two anonymous reviewers whose comments led to a substantial improvement of the manuscript. We thank Y. Kushnir for kindly sharing the data with us which was used to produce Fig. 1. M.E.M. acknowledges support through the NSF Earth Systems History program (ATM-9626833) and the Alexander Hollaender Distinguished Postdoctoral Research Fellowship program of the Department of Energy.

## References

- Allan R, Lindesay J, Parker D (1996) *El Niño Southern Oscillation and climate variability*. CSIRO Publishing, 150 Oxford St. (PO Box 1139), Collingwood, Victoria 2066, Australia
- Allan RJ (1999) ENSO and climatic variability in the last 150 years. In Diaz, HF and V. Markgraf (eds.), *El Niño and the Southern Oscillation: Multiscale variability and its impact on natural ecosystems and society*. Cambridge University Press, Cambridge, UK
- Bjerknes J (1964) Atlantic air-sea interaction. *Advances in geophysics*. Academic Press, New York, pp 1–82
- Capotondi A, Holland WR (1998) Thermohaline circulation variability in the NCAR Climate System Model (CSM). NCAR Technical Note, NCAR/TN-445+STR
- Cubasch U, Voss R, Hegerl GC, Wazskewitz J, Crowley TJ (1997) Simulation of the influence of solar radiation variations on the global climate with an ocean-atmosphere general circulation model. *Clim Dyn* 13: 757–767
- Cullen H, D'Arrigo R, Cook E, Mann ME (2000) Multiproxy-based reconstructions of the North Atlantic Oscillation over the past three centuries. *Paleoceanography* (in press)
- Delworth TL, Greatbatch RJ (2000) Multidecadal thermohaline circulation variability driven by atmospheric surface flux forcing. *J Clim* 13: 1481–1495
- Delworth TL, Manabe S, Stouffer RJ (1993) Interdecadal variations of the thermohaline circulation in a coupled ocean-atmosphere model. *J Clim* 6: 1993–2011
- Delworth TL, Manabe S, Stouffer RJ (1997) Multidecadal climate variability in the Greenland Sea and surrounding regions: a coupled model simulation. *Geophys Res Lett* 24: 257–260
- Deser C, Blackmon M (1993) Surface climate variations over the North Atlantic ocean during winter: 1900–1989. *J Clim* 6: 1743–1753
- Dixon KD, Delworth TL, Spelman MJ, Stouffer RJ (1999) The influence of transient surface fluxes on North Atlantic overturning in a coupled GCM climate change experiment. *Geophys Res Lett* 26: 2749–2752
- Folland CK, Parker DE, Kates FE (1984) Worldwide marine temperature fluctuations 1856–1981. *Nature* 310: 670–673
- Folland CK, Palmer TN, Parker DE (1986) Sahel rainfall and worldwide sea temperatures. *Nature* 320: 602–606
- Folland CK, Owen J, Ward MN, Colman A (1991) Prediction of seasonal rainfall in the Sahel region using empirical and dynamical methods. *J Forecast* 10: 21–56
- Folland CK, Parker DE, Colman A, Washington R (1999) Large-scale modes of ocean surface temperature since the late nineteenth century. In: Navarra A (ed) *Beyond El Niño: decadal and interdecadal climate variability*. Springer, Berlin Heidelberg New York, pp 73–102
- Folland CK, Allan RJ, Mann ME, Power SB (1999) Patterns of large-scale climatic variability in the instrumental era. Proc 22nd General Assembly of the International Union of Geodesy and Geophysics, 18–30 July 1999, Birmingham, UK
- Griffies SM, Tziperman E (1995) A linear thermohaline oscillator driven by stochastic atmospheric forcing. *J Clim* 8: 2440–2453
- Hasselmann K (1976) Stochastic climate models. Part I: theory. *Tellus* 28: 473–485
- Haywood JM, Stouffer RJ, Wetherald RT, Manabe S, Ramaswamy V (1997) Transient response of a coupled model to estimated changes in greenhouse gas and sulfate concentrations. *Geophys Res Lett* 24: 1335–1338
- Hurrell JW (1995) Decadal trends in the North Atlantic Oscillation, regional temperatures and precipitation. *Science* 269: 676–679
- Kaplan A, Cane MA, Kushnir Y, Clement AC, Blumenthal MB, Rajagopalan B (1998) Analyses of global sea surface temperature 1856–1991. *J Geophys Res* 103: 18 567–18 589
- Kushnir Y (1994) Interdecadal variations in North Atlantic sea surface temperature and associated atmospheric conditions. *J Clim* 7: 141–157
- Kushnir Y, Held I (1996) Equilibrium atmospheric response to North Atlantic SST anomalies. *J Clim* 9: 1208–1220
- Kushnir Y, Tourre Y, Rajagopalan B (1997) Decadal and multidecadal variability in Atlantic SST and sea level pressure. Proc Atlantic Climate Variability Meeting, Lamont Doherty Earth Observatory, Columbia University, 24–26 September, 1997
- Lamb PJ, Pepler RA (1987) North Atlantic oscillation: concept and an application. *Bull Am Meteorol Soc* 68: 1218–1225
- Latif M (1998) Dynamics of interdecadal variability in coupled ocean-atmosphere models. *J Clim* 11: 602–624
- Lean J, Rind D (1998) Climate forcing by changing solar radiation. *J Clim* 11: 3069–3094
- Manabe S, Stouffer RJ (1994) Multiple-century response of a coupled ocean-atmosphere model to an increase of carbon dioxide. *J Clim* 7: 5–23
- Manabe S, Stouffer RJ, Spelman MJ, Bryan K (1991) Transient response of a coupled ocean-atmosphere model to gradual changes of atmospheric CO<sub>2</sub>. Part I. Annual mean response. *J Clim* 4: 785–818

- Manabe S, Stouffer RJ, Spelman MJ, Bryan K (1992) Transient response of a coupled ocean-atmosphere model to gradual changes of atmospheric CO<sub>2</sub>. Part II. Seasonal response. *J Clim* 5: 105–126
- Mann ME (2000) Large-scale climate variability and connections with the middle east during the past few centuries. *Climatic Change* (in press)
- Mann ME, Lees J (1996) Robust estimation of background noise and signal detection in climatic time series. *Clim Change* 33: 409–445
- Mann ME, Park J (1994) Global scale modes of surface temperature variability on interannual to century time scales. *J Geophys Res* 99: 25 819–25 833
- Mann ME, Park J (1996) Joint spatio-temporal modes of surface temperature and sea level pressure variability in the Northern Hemisphere during the last century. *J Clim* 9: 2137–2162
- Mann ME, Park J (1999) Oscillatory spatiotemporal signal detection in climate studies: a multiple-taper spectral domain approach. *Adv Geophys* 41: 1–131
- Mann ME, Park J, Bradley RS (1995) Global interdecadal and century-scale oscillations during the past five centuries. *Nature* 378: 266–270
- Mann ME, Bradley RS, Hughes MK (1998) Global-scale temperature patterns and climate forcing over the past six centuries. *Nature* 392: 779–787
- Mann ME, Bradley RS, Hughes MK (1999) Northern Hemisphere temperatures during the past millennium: inferences, uncertainties, and limitations. *Geophys Res Lett* 26: 759–762
- Mann ME, Bradley RS, Hughes MK (2000a) Long-term variability in the El Niño Southern Oscillation and associated teleconnections. In: Diaz HF, Markgraf V (eds) *El Niño and the Southern Oscillation: multiscale variability and its impacts on natural ecosystems and society*. Cambridge University Press, Cambridge, UK (in press)
- Mann ME, Gille E, Bradley RS, Hughes MK, Overpeck JT, Keimig FT, Gross W (2000b) Global temperature patterns in past centuries: an interactive presentation. *Earth Interact* (in press)
- Minobe S (1997) A 50–70 year climatic oscillation over the North Pacific and North America. *Geophys Res Lett* 24: 683–686
- Minobe S (1999) Resonance in bidecadal and pentadecadal climate oscillations over the North Pacific: role in climatic regime shifts. *Geophys Res Lett* 26: 855–858
- Parker DE, Folland CK (1991) Worldwide surface temperature trends since the mid-19th century. In: Schlesinger ME (ed) *Greenhouse-gas-induced climatic change: a critical appraisal of simulations and observations*. Elsevier, Amsterdam, pp 173–193
- Santer BD, Wigley TML, Barnett TP, Anyamba E (1996) Climate change 1995. In: Houghton J, Meira Filho LG, Callander BA, Harris N, Kattenberg A, Maskell K (eds) *climate change 1995: the science of climate change*. Cambridge University Press, Cambridge, UK, pp 407–443
- Schlesinger ME, Ramankutty N (1994) An oscillation in the global climate system of period 65–70 years. *Nature* 367: 723–726
- Stocker TF, Mysak LA (1992) Climatic fluctuations on the century time scale: a review of high-resolution proxy data and possible mechanisms. *Clim Change* 20: 227–250
- Thompson DW, Wallace JM (1998) The Arctic Oscillation signature in the wintertime geopotential height and temperature fields. *Geophys Res Lett* 25: 1297–1300
- Timmermann A, Latif M, Voss R, Grotzner A (1998) Northern Hemispheric interdecadal variability: a coupled air-sea mode. *J Clim* 11: 1906–1931
- Tourre Y, Rajagopalan B, Kushnir Y (1999) Dominant patterns of climate variability in the Atlantic over the last 136 years. *J Clim* (in press)
- Vellinga M, Wood RA (1999) Decadal variability of North Atlantic Deep Water transport in the HADCM3 climate model. Abstract volume from the Fourth Int Conf Modelling of Global Climate Change and Variability, 13–17 September, 1999
- Waple A, Mann ME, Bradley RS (2000) Long-term patterns of solar irradiance forcing in model experiments and proxy based surface temperature reconstructions. *Clim Dyn*, (in press)
- Wood RA, Keen AB, Mitchell JFB, Gregory JM (1999) Changing spatial structure of the thermohaline circulation in response to atmospheric CO<sub>2</sub> forcing in a climate model. *Nature* 399: 572–575